SOLITARY WAVES IN THE EARTH'S UPPER IONOSPHERE

S. H. Kjus, H. L. Pécseli, B. Lybekk, J. Holtet
Physics Department, University of Oslo, Box 1048 Blindern
N-0316 Oslo, Norway
Fax:+47 22 85 56 71
E-mail: s.h.kjus@fys.uio.no
URL (homepage): http://www.uio.no/~skjus/index.html
URL (institution): http://www.fys.uio.no/plasma/index.html

J. Trulsen
Institute for Theoretical Astrophysics, University of Oslo,
Box 1029 Blindern N-0315 Oslo, Norway

A. Eriksson
Swedish Institute of Space Physics, S-755 91 Uppsala, Sweden

Abstract

Localized electrostatic wave packets in the frequency range of lower hybrid waves have been detected by the instruments on the FREJA satellite and earlier also by instrumented rocket payloads. These waves are often associated with local density depletions, indicating that the structures can be interpreted as wave filled cavities which are strongly elongated along the magnetic field. Frequently, the observed wave packets have the appearance of almost textbook illustrations of envelope solitons. The basic features of the observations are presented and discussed.

1 Introduction

Localized electrostatic wave packets in the lower hybrid wave frequency region have been detected by instrumented rockets MARIE as reported by LaBelle et al. [1986] and on TOPAZ III described by Vago et al. [1992], and lately by measurements from the FREJA satellite [Dovner et al., 1994; Eriksson et al., 1994; Dovner et al., 1997]. Instruments on board the FREJA satellite [Lundin et al., 1994] measure wave bursts in the range of several hundred Hz to a few kHz. A sequence of such bursts is shown in Fig. 1, where the two upper panels give the electric field in the *mf*-band (first) and in the *lf*-band. The density perturbation in % is shown in the third and fourth panel, while the magnetic field fluctuations are shown in the lower panel. The *lf*-band is obtained with a sampling rate of 4 kHz, while the *mf*-band is sampled by 16 kHz. A characteristic feature of these events is a density depletion accompanied by an enhancement of the electric field fluctuations, giving the appearance of wave filled cavities in the ionospheric plasma. In Fig. 2 we show an isolated event. Since the plasma index of refraction, η, varies with density, it is evident that the evolution of the wavepacket is accompanied by a corresponding variation in η. The observations have the distinct appearance of an envelope soliton. The observed phenomena seems to be very persistent, thousands of such cavities have been observed.

In the present work we summarize some new results concerning the basic properties of the observed phenomena and some aspects of their interpretation.

2 Occurrence of cavities

A large number of passes was analyzed in order to determine the regions of occurrence for the wave–filled cavities. Table 1 gives a summary of the orbits which were analyzed for the present study. Fig. 3 shows an overview of the polar region where the thin lines indicate the orbits in table 1, while heavy lines indicate regions where cavities were observed. Note that some passes were void of cavities. The present analysis supplements that of Dovner et al. [1997]. Our database is not as complete as theirs, but the presentation of data and scope of analysis is different.

2.1 Basic characteristics of individual wave-packets and cavities

Details of a wave-filled cavity are shown in Fig. 2. Note that the probes detecting the density variations and those measuring electric fields are separated in space, i.e. the observation times of peak density depletion and local wave envelope maxima does not necessarily coincide even in the case that the spatial

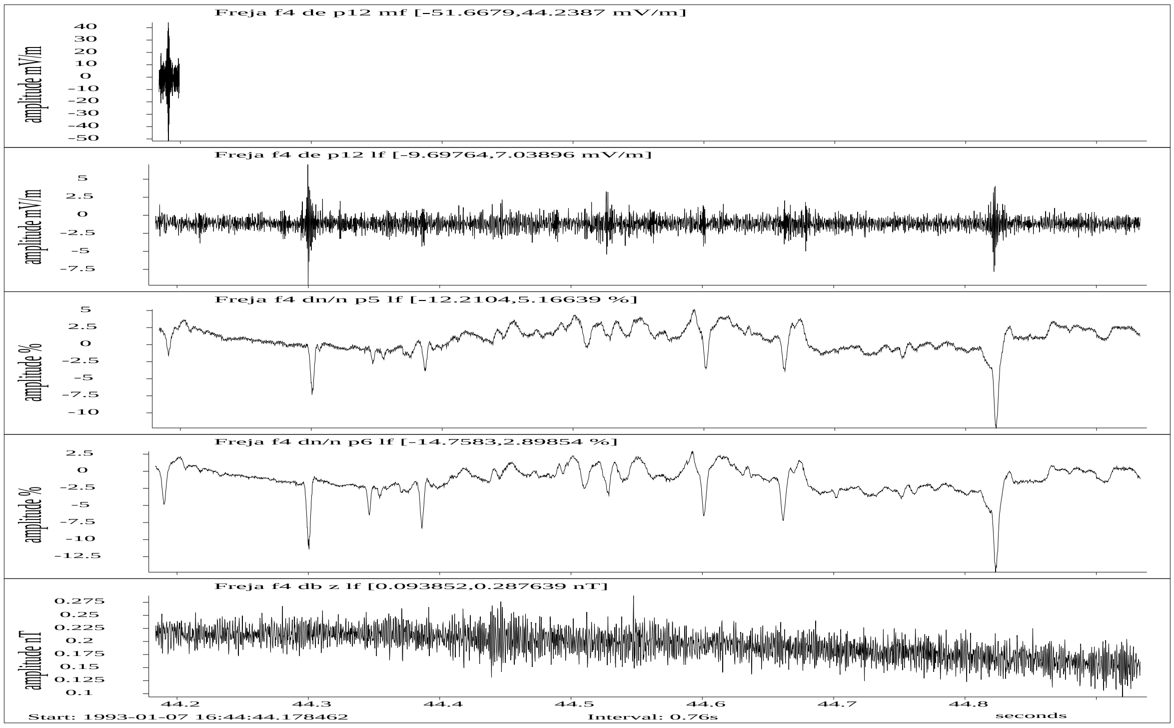

Figure 1: A typical data sequence showing wave activity and density depletions as detected by instruments on the FREJA satellite. The wave electric field in the two upper panels show the high frequency *mf*–band (sampling freq. 16 kHz) (first) and the low frequency *lf*–band (sampling freq. 4 kHz) (second) of the detecting probe circuits. Note that the *lf*–signal here only serves as an indicator for the presence of waves; to obtain the full wave–amplitude the *mf*–signal has to be considered. The *mf*–data are however of shorter time-duration. The third and fourth panel shows the low frequency relative plasma density variations in %, as obtained by Langmuir probes. The reference–level for density fluctuations is set automatically as an average of the entire data sample. The lower panel shows magnetic field fluctuations. Note that the mf-band is here only available in a burst mode of 16 ms duration. (The figure is generated by the ISDAT program.)

wave envelope closely follows the density variation.

Concerning the low frequency density variations, signals are available from *two* Langmuir probes with an 11 m separation. In most cases, a density depletion is observed in *both* signals, see Fig. 1, and it is found that the depletion propagates from one probe to the other, generally with negligible change in shape, indicating that the evolution of density depletions is slow compared to the satellite cavity-transit time [Dovner et al., 1994].

Wave-packets accompanying the density depletions are usually seen in the *lf* as well as *mf* data for the electric fields. Sometimes the signal can be present only in the *mf* band, as shown in an example by Pécseli et al. [1996]. On the other hand there are examples where a clear density depletion was present without any local wave activity, see Pécseli et al. [1996], although unmistakable examples of this type are relatively sparse.

To obtain detailed information of the frequency variation we used a wavelet transform of the electric field data, see also Pécseli et al. [1996]. A typical result is shown in Fig. 2. Since the *mf*–data are usually only available during a burst mode, we can not expect always to have the *mf*–band activity available for a given cavity, but observe the signal to be cut–off as in Fig. 1, top frame. The wave frequency is evidently restricted to a relatively narrow frequency range centered at 4 kHz and the characteristic frequency can be determined quite accurately.

Simultaneous measurements of electric and magnetic field components demonstrate that the fluctuations considered here are electrostatic [Dovner et al., 1994; Eriksson et al., 1994; Pécseli et al., 1996]. By using the ionospheric data for the actual conditions, it is readily demonstrated that the observed frequencies in the spacecraft frame of reference are comparable to the lower hybrid frequency ω_{LH}, and that no other electrostatic waves seem to be likely candidates.

When interpreting the satellite observations, we have to bear in mind that the cavities are spatially localized structures which are intercepted by the satellite orbit at random positions. For instance a cavity width determined from one observation is just a chord length and not necessarily the diameter of the actual cavity. Although it is not logically possible to draw any conclusion concerning the full space

Table 1: Summary of the orbits used in the present analysis. The time–periods with cavities are noted explicitly.

Orbit	Date	Time (UT)	CGLat/Long	Observed cavities
0785	1992-12-04	17:16 - 17:41	55/-33 – 48/74	none
0790	1992-12-05	02:23 - 02:49	54/-164 – 53/-56	02:33:00 - 02:33:37
0795	1992-12-05	11:24 - 11:40	49/53 – 60/113	none
0803	1992-12-06	01:59 - 02:25	53/-163 – 54/-54	none
0984	1992-12-19	18:31 - 18:55	39/-123 – 70/-39	18:50:28 - 18:51:54 (few)
1234	1993-01-07	16:38 - 17:03	49/-148 – 61/-42	16:42:45 - 16:46:53 and 16:56:41 - 16:57:53
1273	1993-01-10	15:25 - 15:51	44/-146 – 63/40	15:34:45 - 15:38:33 and 15:51:17 - 15:51:21
1547	1993-01-31	09:14 - 09:32	73/-80 – 45/00	09:23:58 - 09:28:42
1572	1993-02-02	06:35 - 06:56	69/-58 – 44/33	06:42:10 (few)
1640	1993-02-07	09:57 - 10:22	50/-153 – 59/-46	10:21:02 - 10:22:30
1694	1993-02-11	12:09 - 12:35	61/-169 – 45/-72	12:18:03 (few)
1728	1993-02-14	01:49 - 02:12	62/-43 – 47/58	01:56:15 - 01:56:32 (few)
1772	1993-02-17	09:45 - 10:11	57/-167 – 50/-62	10:08:30 - 10:09:46
1963	1993-03-03	20:32 - 20:56	55/-33 – 49/71	20:48:55 - 20:51:43
2112	1993-03-15	03:09 - 03:35	55/-164 – 52/-57	03:12:14 - 03:13:22 and 03:25:58 - 03:26:54
2152	1993-03-18	03:51 - 04:17	60/-169 – 46/-71	03:51:24 - 03:52:24
2569	1993-04-18	16:56 - 17:22	47/-149 – 60/-41	17:03:46 - 17:05:06
4533	1993-09-14	07:24 - 07:49	53/-157 – 56/-51	none
6663	1994-02-22	11:09 - 11:30	65/-45 – 46/48	11:09:08 - 11:10:26 (few) and 11:18:06 - 11:22:52
7580	1994-05-02	20:14 - 20:34	70/-52 – 43/32	20:13:10 - 20:13:14 and 20:16:42 - 20:21:28
7593	1994-05-03	19:49 - 20:10	68/-61 – 44/34	19:50:17 - 19:52:59 and 19:55:21 - 19:57:07

time variation of the individual cavities observed, it is nevertheless meaningful to propose a physically realistic model for the space time evolution of cavities, and by simple assumption on the statistics on the intersection of cavities by the satellite, the relevant statistical distributions of cavity widths and other parameters can be determined. These analytically obtained distributions can then be compared to the experimental ones and the model accepted or rejected according to the agreement between the two. In this way it is possible to obtain some "average" information which in some sense pertains also to the individual cavities.

In the first analysis of this kind for the present data, Pécseli et al. [1996] studied the collapse model often suggested (e. g. by Shapiro et al. [1993]) as a likely explanation for the occurrence of lower hybrid wave cavities. In this study the time evolution of the cavity width was assumed to be prescribed by the analytic results from collapsing lower hybrid waves. Assuming the collapse to be initiated at random, uniformly distributed times an expression for the cord–length distribution was obtained to be compared with experimental results. Although the study assumed a simple "inverted top hat" model for the density depletions, the results were rather unambiguously speaking against the proposed model. An alternative to the collapse model was suggested in terms of a thermal instability as discussed in detail by Pécseli et al. [1996]. Here, the waves give up energy to particles predominantly in positions where a small density depletion is present due to some random irregularity. Due to the local pressure increase the plasma subsequently expands along the magnetic field lines and the process results in an enhancement of the original irregularity and an ensuing local trapping of the lower hybrid wave.

As an extension of the analysis by Pécseli et al. [1996, 1997] we show in Fig. 4 a scatterplot for the simultaneously measured peak amplitudes and widths, obtained from the data. By inspection it is evident that large density depletions are in general also those with the largest spatial width. This is clearly in contradiction with a collapse model where the cavities are initially wide and shallow, and subsequently narrows while the density is depleted. The scatter in the data points in Fig. 4 can have two different origins: either the cavities are all more or less identical and the scatter arises because of the statistical variation in the orbits along which they are sampled by the satellite. Alternatively, the scatter is predominantly reflecting the statistical distribution in the scales of the many cavities. This question can again only be resolved by postulating a model, derive its statistical properties and compare these with observations. We here assume that the time evolution of the cavity is so slow that its variation during the transit time of the satellite can be ignored. This seems to be a good approximation since the cavities are usually found to be symmetric, see e. g. Fig. 2, i. e. the gradients on two sides of the density depletions are the same. This property can only be explained by the assumed slow time evolution. Then we postulate an analytical form

$$n = n_0 - \Delta n \, e^{-\frac{1}{2}[(x^2+y^2)^m/R^{2m}]} \, . \qquad (1)$$

With the adjustable parameters m, R and Δn, the model can accommodate a large variety of cavity forms. The inverted top hat model referred to before is obtained for $m \to \infty$, while a simple exponential density depletion is found for $m = 1$. We use the same exponent on both x and y for symmetry reasons, since the problem does not have any

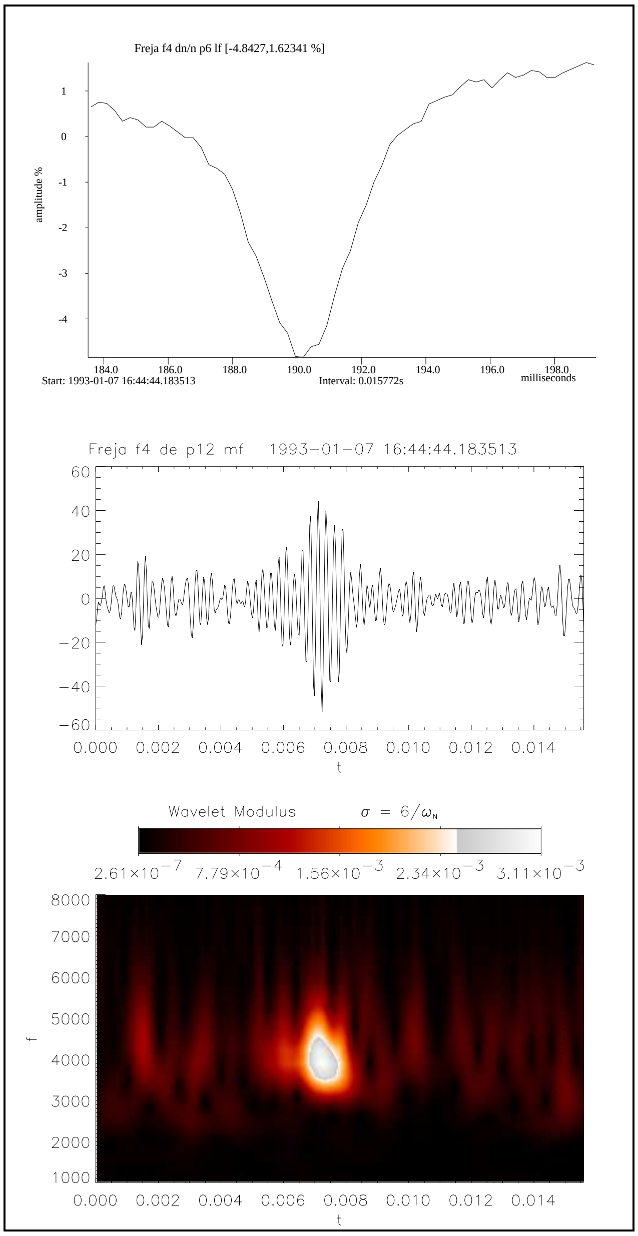

Figure 2: Examples of lower hybrid wave cavities detected by instruments on the FREJA satellite. The upper panel is the relative plasma density variations in %, the middle panel is the electric field fluctuation in the *mf*-band and the lower panel shows the wavelet transform of the electric field fluctuations. The wavelet analysis is based on a Morlet wavelet. Note that the probes detecting density and electric fields are at different spatial positions on the satellite. This gives rise to a slight relative displacement of the respective signals.

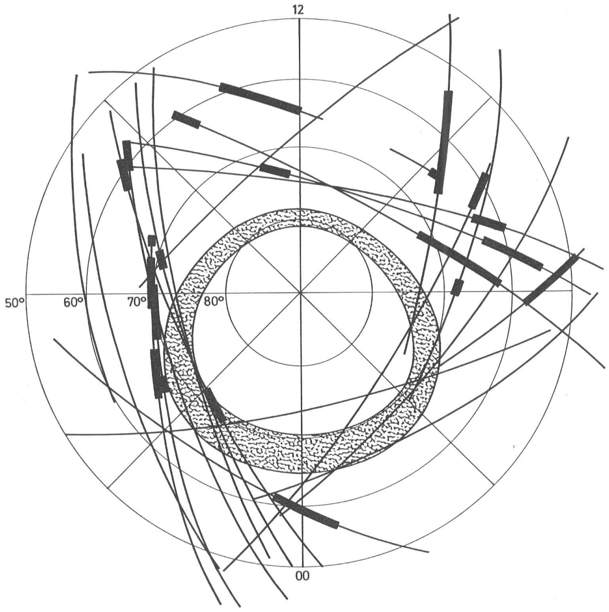

Figure 3: Survey of occurrences of wave filled cavities as obtained by analyzing the orbits listed in table 1. Heavy line indicates time–intervals where cavities were observed. An average auroral oval is included in the figure for reference.

preferred direction perpendicular to a locally homogeneous magnetic field and when large scale density gradients are of minor importance. In (1) we can take $y =$ const. as an impact parameter defining the distance between the satellite orbit and the center of the cavity, while x is the coordinate along the satellite trajectory which in the data is translated into a time–variable $t = x/V$ with V being the satellite velocity.

The result (1) offers a straight forward parametric presentation of the normalized depth–chordlength relation as

$$\left\{ e^{-\frac{1}{2}(\xi)^{2m}}, 2\sqrt{\sqrt[m]{2\ln 2 + (\xi)^{2m}} - (\xi)^2} \right\} \qquad (2)$$

with $\xi \equiv y/R$ being the normalized impact parameter, and the density perturbation being normalized by its peak value. The cordlength in (2) is defined at the halfvalue of the peak amplitude, $\exp\left(-\frac{1}{2}\xi^{2m}\right)$, along the trajectory.

When examining an actual record, the impact parameter is in general varying from cavity to cavity, with y being statistically distributed. The only acceptable assumption concerning its probability density is a uniform distribution, $P(y) = 1/L_M$ for $0 < y < L_M$, and zero otherwise, where L_M is a maximum distance of the satellite from the center of a cavity. Eventually we let $L_M \to \infty$. With this assumption we can in principle easily obtain the marginal probability densities $P(\ell)$ and $P(\tilde{n})$. For instance, using $P(\tilde{n})d\tilde{n} = P(y)dy$ we readily find

$$P\left(\frac{\tilde{n}}{\Delta n}\right) = \frac{1}{2mL_M}\frac{\Delta n}{\tilde{n}}\left[\ln\left(\frac{\tilde{n}}{\Delta n}\right)\right]^{-1+1/(2m)}, \tag{3}$$

with $e^{-\frac{1}{2}(L_M/R)^{2m}} < \tilde{n}/\Delta n < 1$. The probability density (3) is normalized for all finite L_M, but the expression may give trivial results in the limit of $L_M \to \infty$ for certain m.

We can test (1) by fitting the parameters m and R to the actual data. As an illustration we show in Fig. 5 such a fit obtained for the cavity shown in Fig. 2. The data from the two probes are shown with black dots given with the low frequency sampling used in this case, while the full line is a Gaussian, i. e. $m = 1$, while $R = 0.0016$ s, corresponding to a length scale of 9.7 m. Note that the *same* Gaussian is used for both signals, since it is the same cavity which is intercepted at two position by the two Langmuir probes. Evidently, the fit is quite good in this case. We have examined a number of cavities and find that a Gaussian can be used as a good approximation in a number of cases (although not always). This observation indicates that $m \approx 1$ is a useful approximation when analyzing the data. In this case, however, the relation (2) becomes particularly simple, giving $\left\{e^{-\frac{1}{2}(\xi)^2}, 2\sqrt{2\ln 2}\right\}$. With y being statistically distributed, but all cavities identical, the scatterdiagram in Fig. 4 should give one vertical line with all chord–lengths being the same and identical to the cavity half–width. Evidently this is not the case, and we can conclude that the cavity diameters are statistically distributed, with distributions as those shown by Pécseli et al. [1996], for instance. The intuitive conclusion reached by inspection of Fig. 4 is confirmed, i. e. the most shallow density depletions are likely to be the most narrow ones. The arguments against a collapse model are strengthened by the present analysis.

2.2 Conditions for occurence of cavities

We note from Fig. 3 that the distribution of regions containing cavities is not uniform on the polar region. There are regions with several orbits but with few or no cavity observations. On the other hand there are regions where cavities are present in every orbit. To give an indication for the origin of this seemingly uneven spatial distribution of cavities we show in Fig. 6 a summary figure from Hartz [1971] giving the distribution of precipitating particles in the northern hemisphere. The *drizzle–type* high energy auroral–zone precipitation seems to have a distribution reminiscent of the cavity distribution we observe. Although the statistics need to be improved, this agreement deserves a closer scrutiny.

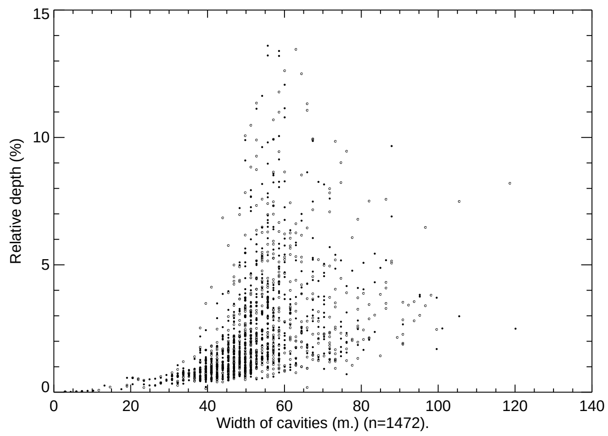

Figure 4: Scatterdiagram for amplitudes and chord–lengths obtained for cavities found in one satellite pass. The vertical "stripes" arise because of the sampling in the data.

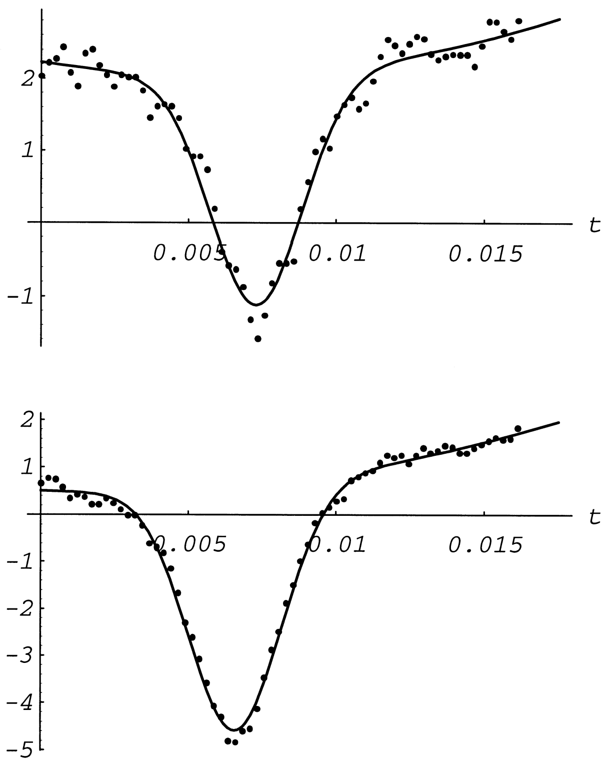

Figure 5: Fit of a Gaussian for one selected cavity. The two curves correspond to the two Langmuir probes which intercept the cavity at two different positions. In the curve–fitting we allowed also for two small terms proportional to t and t^2. Being small corrections, these were not included in the analysis.

Using the data for electron and ion energy distributions obtained on the satellite we can attempt to correlate the occurrence of cavities with these observations. Examples are shown in Fig. 7, where energy spectra as functions of time are presented for electrons and various ions. A horizontal bar at the bottom of the figure indicate the time–interval where cavities were observed. See also Dovner et al. [1997] for a similar figure taken at a different orbit. To complete the presentation we considered also data for magnetic fields and currents. No straight forward or evident conclusion emerges from these and similar studies. Usually we find cavities present in the vicinity, or just outside, regions of enhanced magnetospheric activity, where strong conductivity gradients are expected.

A conclusion which is consistent with the observations can be made as follows. It can be argued that the active regions are characterized by excitation of many different wavetypes, which can disturb the formation of cavities *inside* these regions. It thus seems difficult to imagine formation of cavities in an environment with significant activity of ion–acoustic waves, for instance. Cavities are thus assumed to be excited in the regions with drizzle–type particle precipitation, but quenched in the active regions as argued. We expect that lower–hybrid waves can be excited as well in these active regions. All these different wavetypes are radiated out of these active regions, and most of them will be damped. Lower–hybrid waves propagating perpendicular to magnetic fields are however without any noticeable linear damping, see for instance the numerically obtained linear dispersion relation given by Pécseli et al. [1996]. Outside the active regions these waves can generate cavities without the disturbance or interference from other wavetypes. By the latter argument the active regions are important for the generation of lower–hybrid waves, explaining a preference for observing waves in the vicinity of such regions. It can however not be argued that such active regions are the *only* sources of lower–hybrid waves.

A possible correlation between areas of cavities and the Kp-index is also investigated, but there seems to be no correlation.

2.3 Spatial distribution of cavities

Two different scenarios for the formation of cavities can be distinguished; one where they are generated with more or less regular intervals (for instance by a modulational instability) or alternatively by a random process where a cavity is formed at a spatial position independent of the presence of others. These, or other, conjectures can be tested experimentally.

We propose, as a hypothesis, that the cavities are randomly distributed along the spacecraft trajectory, with the position of one cavity being statistically independent of all others [Pécseli et al., 1996; Pécseli et al., 1997]. The consequence of the hypothesis is that cavities are to be Poisson distributed along the trajectory, i.e. the distribution of the number N of cavities in an interval of length $\mathcal{L}$ is $P(N) = (\nu\mathcal{L})^N \exp(\nu\mathcal{L})/N!$ with ν being the density of cavities along the trajectory. An estimate for this probability density is a measurable quantity, offering a straight forward test of the hypothesis. Here we took the time interval to be 0.375 s, corresponding to a spatial interval of $2.33 \cdot 10^3$ m. As a check we also considered other durations of the time interval, see also Pécseli et al. [1997]. Results are shown in Fig. 8, based on data for plasma density, supported by lf–data, taking into account that not *all* cavities need to have a noticeable wave activity in the lf–band. The identification of cavities is not straight forward in all cases, but the uncertainty is expected to diminish in significance when a large number of events are analyzed. A Poisson distribution is found to be reasonably justified.

An alternative test of the Poisson hypothesis is to obtain the distribution of separation between cavities. For the Poisson model the distribution should follow an exponential, with the exponent determining the average distance between cavities along the satellite trajectory. This analysis was carried out with results shown in Fig. 9 and the average distance between cavities given in table 2.

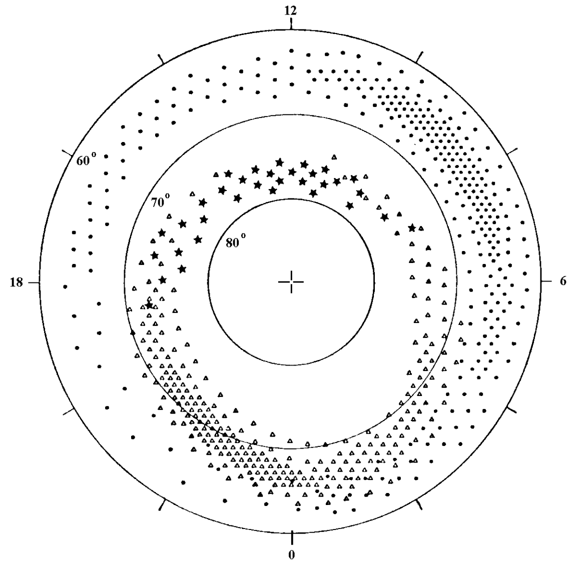

Figure 6: Survey of particle precipitation in the northern hemisphere. The auroral oval (medium–energy) precipitation (splash–type) is represented by triangles, the auroral zone (high–energy) precipitation (drizzle–type) by the dots, and the polar cusp (low–energy) precipitation on the day side by asterisks. The approximate average flux is indicated by the density of symbols. The figure is adapted from Hartz [1971].

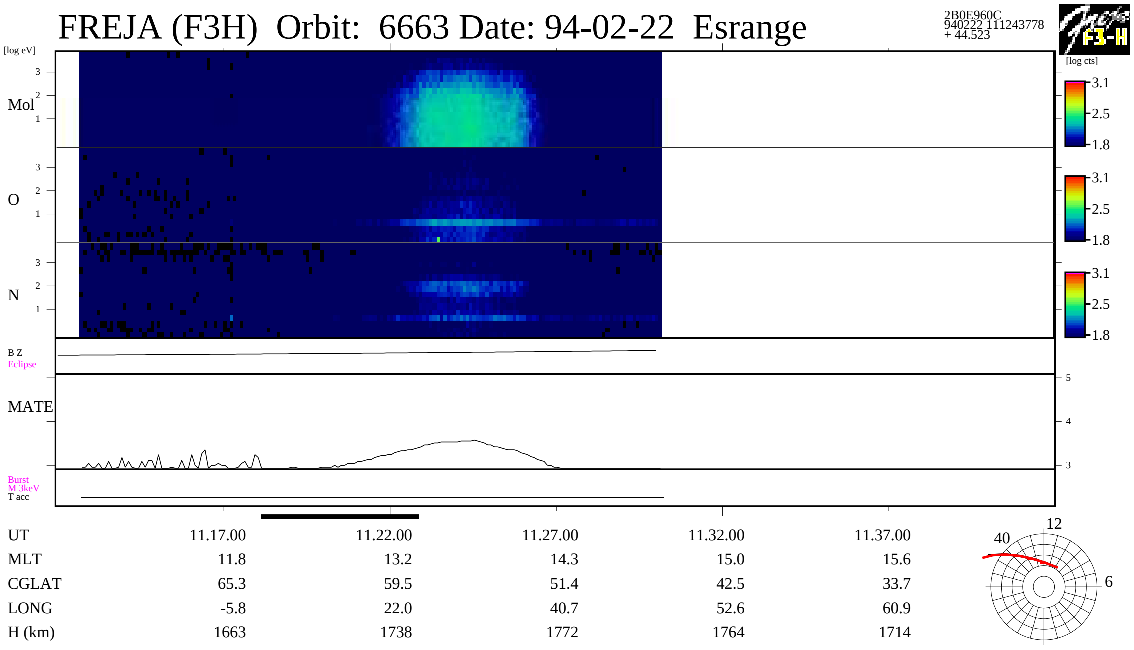

Figure 7: Particle energy distributions as functions of time. A horizontal bar below the figure indicate the time–interval where cavities were observed. The notation *Mol* refers to ions heavier than O^+, while *MATE* is for the high energy electron spectrometer.

Table 2: Characteristic quantities of lower hybrid waves and cavities.

Typical electric field frequency:	$\sim$ 4 kHz
Average relative plasma density inside a cavity:	$\sim$ 2.1 % below the average density
Average width of cavity:	$\sim$ 54 m
Average distance between cavities:	$\sim$ 350 m
Lengths of intervals containing cavities:	10 km - 1500 km
Altitude range where cavities are detected:	1570 - 1770 km

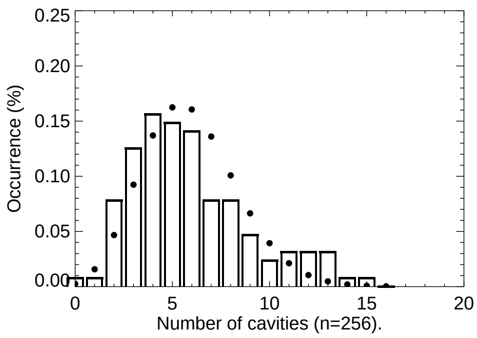

Figure 8: Estimate for the probability density of the number N of cavities in a selected interval of 0.375 s, corresponding to $\mathcal{L}$=2330 m along the space craft trajectory. Data from the pass 1547 were used, see table 1. Black dots are the results for a Poisson distribution. The density of cavities along the satellite trajectory is ν= $2.54{\cdot}10^{-3}$ m^{-1}. The observation is based on 256 cavities. In translating temporal intervals to spatial intervals we used a satellite velocity of 6.2 km/s perpendicular to **B**. The average distance between cavities is $1/\nu$.

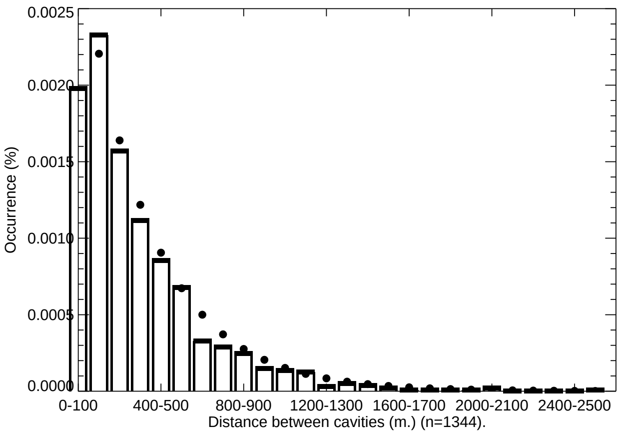

Figure 9: Distribution of distance between cavities corresponding to Fig. 8. The Poisson model would imply this distribution to be an exponential, as indicated by black dots.

3 Conclusions

In this paper we presented some basic properties of the localized bursts of lower hybrid waves and associated density cavities observed by the FREJA satellite. We found indications that the cavities might occur predominantly in regions where we have auroral zone (high–energy) particle precipitation (drizzle–type). There seems to be solid evidence for claiming that cavities are Poisson–distributed in the regions where they occur, and on the basis of this observation it can be argued that cavities develop independently, presumably triggered by some burst type phenomena. Our studies demonstrate that the observed distributions are surprisingly constant in time. For instance the spatial density of cavities varies by less than a factor 3 for data obtained by more than a years separation. These results indicate that lower–hybrid waves and wave cavities are common in the Earth's upper ionosphere, and not necessarily associated with violent events. The occurrence does not have any evident seasonal variation, and within the lifetime of the FREJA satellite, the cavities were present at all years with equal probability. It might be that the lower hybrid wave cavities described in the present study represent the example of solitary wave structures to occur most abundantly in nature.

At times where the cavity activity is significant, the data give a typical density of cavities of $\mu_c \sim 10^{-4}$ m^{-2} in a plane perpendicular to the magnetic field (μ_c has dimensions $length^{-2}$). With an average diameter of 60 m, the cavities cover 10–20 % of the plane.

In a forthcoming paper we attempt give a more detailed discussion of the quantities mentioned here. One important remaining question concerns the elongation of cavities along the magnetic field. Our expectations are that the cavities are long, probably more than several km. A complete energy–budget of the observed lower–hybrid waves is only feasible when this **B**–parallel scale–length is known.

Acknowledgments

This work was in part supported by the Norwegian National Science Foundation. We thank Hermann Lühr at GeoForschungsZentrum, Potsdam, Germany for valuable discussions. We also thank Liv Larssen at the Auroral Observatory at the University of Tromsø for her kind assistance with preparation of some of the figures.

References

Dovner, P. O., Eriksson, A. I., Boström, R. and Holback, B. [1994]. FREJA multiprobe observations of electrostatic solitary structures, *Geophys. Res. Lett.* **21**: 1827.

Dovner, P. O., Eriksson, A. I., Boström, R., Holback, B., Waldemark, J., Eliasson, L. and Boehm, M. [1997]. The occurrence of lower hybrid cavities in the upper ionosphere., *Geophys. Res. Lett.* **24**: 619.

Eriksson, A., Holback, B., Dovner, P. O., Boström, R., Holmgren, G., André, M., Eliasson, L. and Kintner, P. M. [1994]. FREJA observations of correlated small–scale density depletions and enhanced lower hybrid waves, *Geophys. Res. Lett.* **21**: 1843.

Hartz, T. R. [1971]. *The Radiating Atmosphere*, Reidel, Dordrecht.

LaBelle, J., Kintner, P. M., Yau, A. W. and Whalen, B. A. [1986]. Large amplitude wave packets observed in the ionosphere in association with transverse ion acceleration, *J. Geophys. Res* **91**: 7113.

Lundin, R., Haerendel, G. and Grahn, S. [1994]. The FREJA project, *Geophys. Res. Lett.* **21**: 1823.

Pécseli, H. L., Iranpour, K., Holter, Ø., Lybekk, B., Holtet, J., Trulsen, J., Eriksson, A. and Holback, B. [1996]. Lower hybrid wave cavities detected by the FREJA satellite, *J. Geophys. Res.* **101**: 5299.

Pécseli, H. L., Lybekk, B., Trulsen, J. and Eriksson, A. [1997]. Lower–hybrid wave cavities detected by instrumented spacecrafts., *Plasma Phys. Contr. Fusion* **39**: A227.

Shapiro, V. D., Shevchenko, V. I., Solov'ev, G. I., Kalinin, V. P., Bingham, R., Sagdeev, R. Z., Ashour-Abdalla, M., Dawson, J. and Su, J. J. [1993]. Wave collapse at the lower hybrid resonance, *Phys. Fluids* **B5**: 3148.

Vago, J. L., Kintner, P. M., Chesney, S. W., Arnoldy, R. L., Lynch, K. A., Moore, T. E. and Pollock, C. J. [1992]. Transverse ion acceleration by lower hybrid waves in the topside auroral ionosphere, *J. Geophys. Res.* **97**: 16935.